Application of 3D source deghosting and designature to deep-water ocean bottom node data

Xu Li, Jing Yang, Hui Chen, Melanie Vu, and Ping Wang (CGG)*

Summary

Compared to towed-streamer data, deep-water ocean bottom node (OBN) data by nature have a broader bandwidth; however, the presence of the source ghost and source signature can reduce the useful frequency range and therefore decrease seismic resolution. Deep-water OBN data are typically well sampled in the common-receiver domain; thus, the source-side wave-propagation angles can be obtained through plane-wave decomposition for 3D source deghosting and designature. We compared two methods for broadening the bandwidth of deep-water OBN data: (1) 3D source deghosting that assumes a single-point source and (2) 3D joint source deghosting and designature that takes into account the full source-array geometry. Using Gulf of Mexico (GOM) OBN data, we demonstrated that 3D source deghosting effectively removed the source ghost to provide images with a wider spectrum and a better signal-to-noise ratio (S/N). We also found that joint 3D source deghosting and designature can further increase the bandwidth compared to 3D deghosting alone.

Introduction

OBN data have been used for field development planning, reservoir surveillance, and imaging complex structures because OBN geometries can provide full-azimuth coverage, high-fold, broad bandwidth, and a low noise content. Deep-water OBN data inherently have a broader bandwidth because the receiver-side ghost (down-going wavefield) is well separated from primaries (up-going wavefield). However, the source-side ghost and signature still exist in deep-water OBN data and thus limit the frequency bandwidth.

Many deghosting algorithms have been developed for marine seismic data (Kemal et al., 2008; Riyanti et al., 2008; Wang et al., 2013, 2014; Poole, 2013). Wang et al. (2014) proposed a 3D deghosting method that is effective for full-azimuth data with strong 3D effects and has been successfully applied to full-azimuth and ultra-long offset marine towed-streamer data for receiver deghosting (Wu et al., 2014). This algorithm is also well-suited for 3D source deghosting of deep-water OBN data because OBN data are naturally in the common-receiver domain. All the aforementioned deghosting algorithms assume single-point receiver and/or source locations.

For source designature, a common practice is to apply a single 1D filter (zero-angle approximation) to remove the source-side signature. 3D source designature methods that take into account the effect of the air-gun array geometry have also been proposed (Lee et al., 2014; Poole et al., 2015; Wang et al., 2015).

3D source deghosting using a single-point source approximation is often reasonable for regular single-level air-gun array geometries. To accurately account for source directivity, similarly to 3D source designature, source deghosting needs to consider the air-gun array geometry as well. In addition, for complex array geometries such as multi-level source arrays (Siliqi et al., 2013), the effect of the source array geometry for both source deghosting and designature must be considered. Thus, Wang et al. (2015)

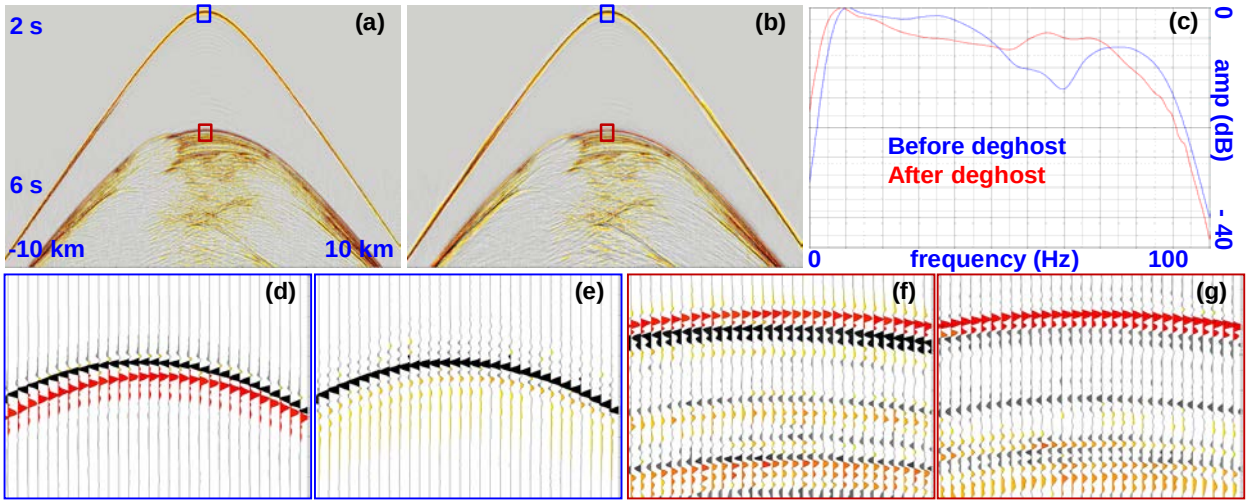

Figure 1: OBN common node gather (a) before deghosting and (b) after deghosting. (c) Amplitude spectrum. The blue curve represents the input data; the red curve is after deghosting. Zoomed-in wavelet view for direct arrival at apex of gather (d) before deghosting and (e) after deghosting. Zoomed-in wavelet view for the water bottom at apex of a gather (f) before deghosting and (g) after deghosting.

DOI http://dx.doi.org/10.1190/segam2015-5924634.1

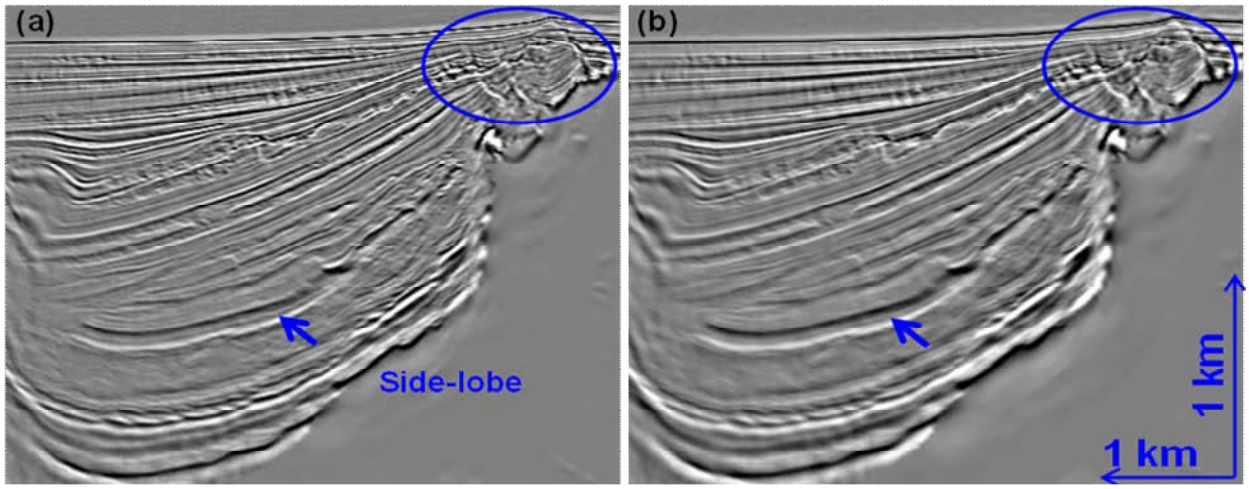

Figure 2: Reverse time migration stack image from OBN data. (a) Inline direction before deghosting. (b) Inline direction after deghosting.

proposed a joint 3D source deghosting and designature method that takes into account the effect of the air-gun array geometry for simultaneous source deghosting and designature. Using synthetic data, they demonstrated that this algorithm effectively removed the source ghost and signature of deep-water OBN geometry in one step.

Using a deep-water OBN data example from the GOM, we demonstrate the effectiveness of 3D source deghosting and compare it with the proposed joint 3D deghosting and designature method.

3D deghosting of deep-water OBN data

Compared to towed-streamer acquisition, OBN geometries often favor 3D source deghosting for two reasons. First, OBN data is naturally in the common-receiver domain, which is an ideal domain for source-side deghosting. Second, deep-water OBN data have a more balanced shot spacing (vs. receiver spacing of towed-streamer data) in both the x and y directions as well as full azimuthal shot coverage. Therefore, deep-water OBN data are generally less spatially aliased for high-frequency content during 3D Tau-P_x-P_y transforms. Therefore, applying 3D deghosting for source deghosting of OBN data will theoretically provide a more accurate result compared to source deghosting of towed-streamer data using shot gathers as input (Wang et al., 2015).

We applied 3D deghosting to an OBN down-going data set from the GOM. The data set was acquired with a constant source depth of 12 m, a notch frequency at approximately 62.5 Hz, and a shot spacing of 50 × 40 m. Figures 1a and 1b show the OBN down-going wavefield node gather before and after 3D deghosting, respectively. A 1D shot-by-shot designature filter (Poole et al., 2013) was applied to the input data. Figure 1c shows the spectrum comparison for the corresponding gather before and after 3D deghosting. More low-frequency energy was boosted, and the source-ghost notch was filled after deghosting. Figures 1d-1g show a zoomed in wavelet view of the direct arrival and the water bottom at the apex of the node gather. The primary and ghost wavelets were easy to identify before deghosting (Figures 1d and1f), and the shot ghost energy was greatly removed after 3D deghosting (Figures 1e and 1g).

To better evaluate the deghosting effect, we applied 35 Hz reverse time migration (RTM) to the data set. The RTM stack images of the basin are shown in Figures 2a (before deghosting) and 2b (after deghosting). One of the benefits of OBN data is that the ghosts were not readily visible even before deghosting—because there was no receiver-side ghost. Nevertheless, after 3D deghosting, the side-lobes due to source ghost was reduced (blue arrows), and the faults had better definition due to better low frequency signals after source deghosting (blue circles). The amplitude spectrum (Figure 3) demonstrated that 3D deghosting provided a broader frequency bandwidth.

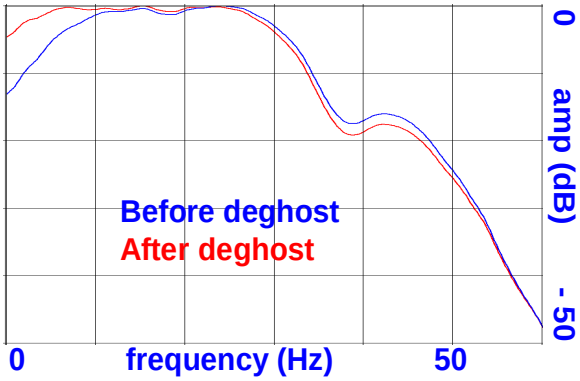

Figure 3: Spectra before and after 3D deghosting.

DOI http://dx.doi.org/10.1190/segam2015-5924634.1

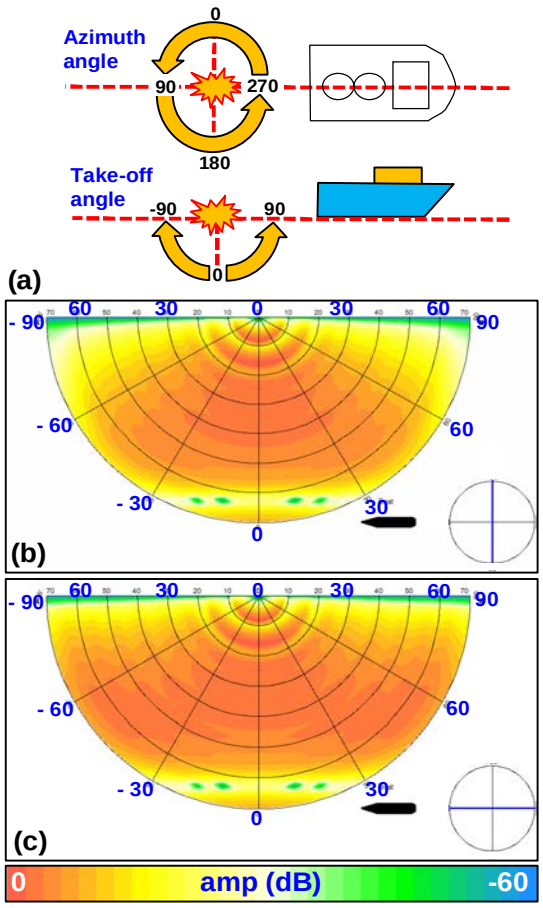

Figure 4: (a) The definition for azimuth and take-off angle in this acquisition. 90° and 270° are parallel to shooting direction; 0° and 180° are perpendicular to the shooting direction. The modeled source directivity with different take-off angles at azimuthal angles of (b) 0°/180° and (c) 90°/270°, respectively.

Joint 3D deghosting and designature

An ideal single-point source was assumed for the 3D deghosting method in the previous section. However, to accurately handle the source deghosting and designature—especially the latter—the source-array geometry and notional sources of airguns must be taken into account. The source array for the OBN data consisted of 21 air-gun clusters with a total volume of 5220 cubic inches. Figure 4a shows the definition of the azimuth and take-off angles in the acquisition. Figures 4b and 4c shows the modeled source directivity patterns for different take-off angles for 0° (Figure 4b) and 90° (Figure 4c) azimuths. For the 0° azimuth, when the take-off angle was beyond 60°, the source directivity started to vary; for the 90° azimuth, the spectrum varied beyond the 75° take-off angle.

According to Ziolkowski et al. (1982), the notional source signatures of each airgun position in the source array can be derived using near-field hydrophone measurements. Far-field signatures in any direction may then be derived using those notional sources. Figures 5a presents the wavelets of directional far-field signatures for 0° azimuth with take-off angles ranging from 0° to 60°. Figure 5b shows the wavelets from 0° to 90° azimuths for take-off angle equal to 30°. Figure 5c shows the spectral comparison of six take-off angles. Figure 5d shows the spectral comparison of nine azimuth angles. Our data had stronger variations with different take-off angles and weaker variations with different azimuth angles. With 1D methods, the far-field signature at a 0° take-off angle is used to design the 1D designature filter, which is insufficient to account for far-field variations with azimuth and take-off angles. To better account for the source directivity of the source-array geometry, we applied the joint 3D deghosting and designature method proposed by Wang et al. (2015).

The input data was the down-going wavefield that already had the 1D debubbling filter applied to it with the source directivity untouched. Figures 6b-6d show a zoomed-in wavelet view of the input, after 3D deghosting, and after joint 3D deghosting and designature, respectively. Figure 6e shows the spectrum comparison after deghosting. The output spectrum after joint 3D deghosting and designature was broader, and the high-frequency energy was better boosted compared to 3D deghosting alone.

Conclusions and discussion

Theoretically, both 3D source deghosting and joint 3D source deghosting and designature require the input data to be in the receiver domain. Deep-water OBN data are naturally acquired in this domain, which is ideal for both methods. Using deep-water OBN data from the GOM, we demonstrated that the 3D deghosting effectively removed ghost energy and joint 3D deghosting and designature attenuated source ghost and signature in one pass while providing a broader bandwidth than 3D deghosting alone.

While 3D deghosting alone assuming a single-point source is applicable to most deep-water OBN data (with constant air-gun depths) for source deghosting, joint 3D source deghosting and designature requires the knowledge of the air-gun array geometry and the notional source signatures of each air-gun that can be derived from near-field hydrophone measurements. For deep-water OBN surveys without such information, we can choose to perform 1D source designature and 3D source deghosting.

Acknowledgements

We thank Kawin Nimsaila and Suryadeep Ray for optimizing the algorithms and Tony Huang for fruitful discussions. We also thank Chevron and CGG for permission to publish this work.

DOI http://dx.doi.org/10.1190/segam2015-5924634.1

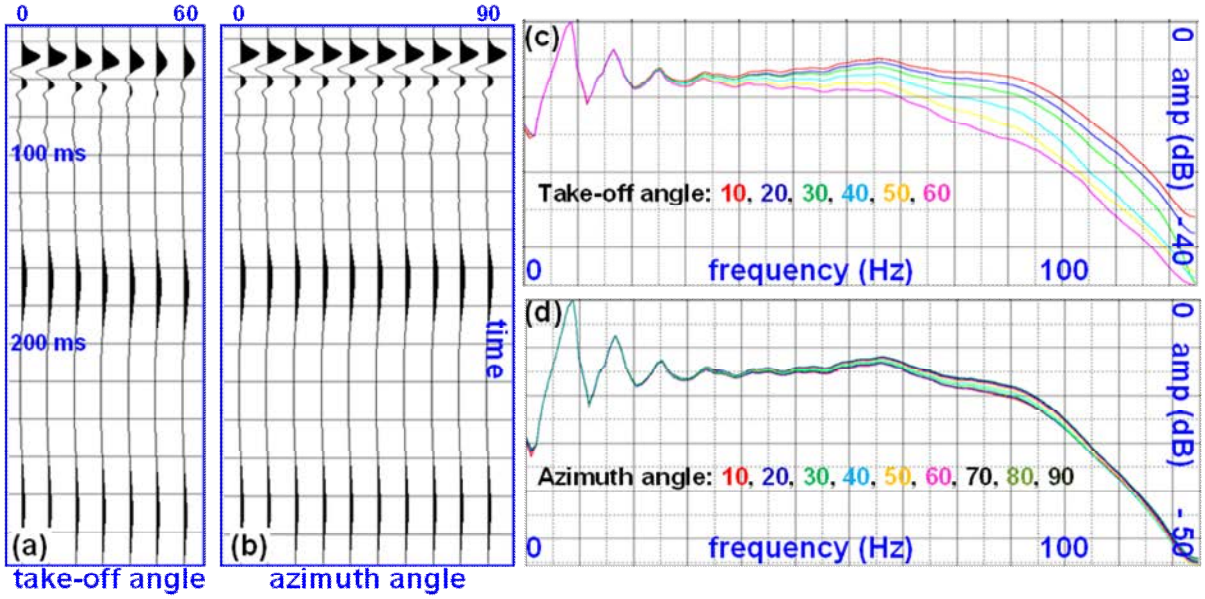

Figure 5: Directional far-field signatures derived from near-field hydrophone. (a) Directional far-field signatures vs. take-off angle for 0° azimuth. (b) Directional far-field signatures vs. azimuth for a take-off angle of 30°. (c) Spectra of different take-off angles (measured over azimuth angles from 0° to 90°). (d) Spectra of different azimuth angles (measured over take-off angles from 0° to 60°).

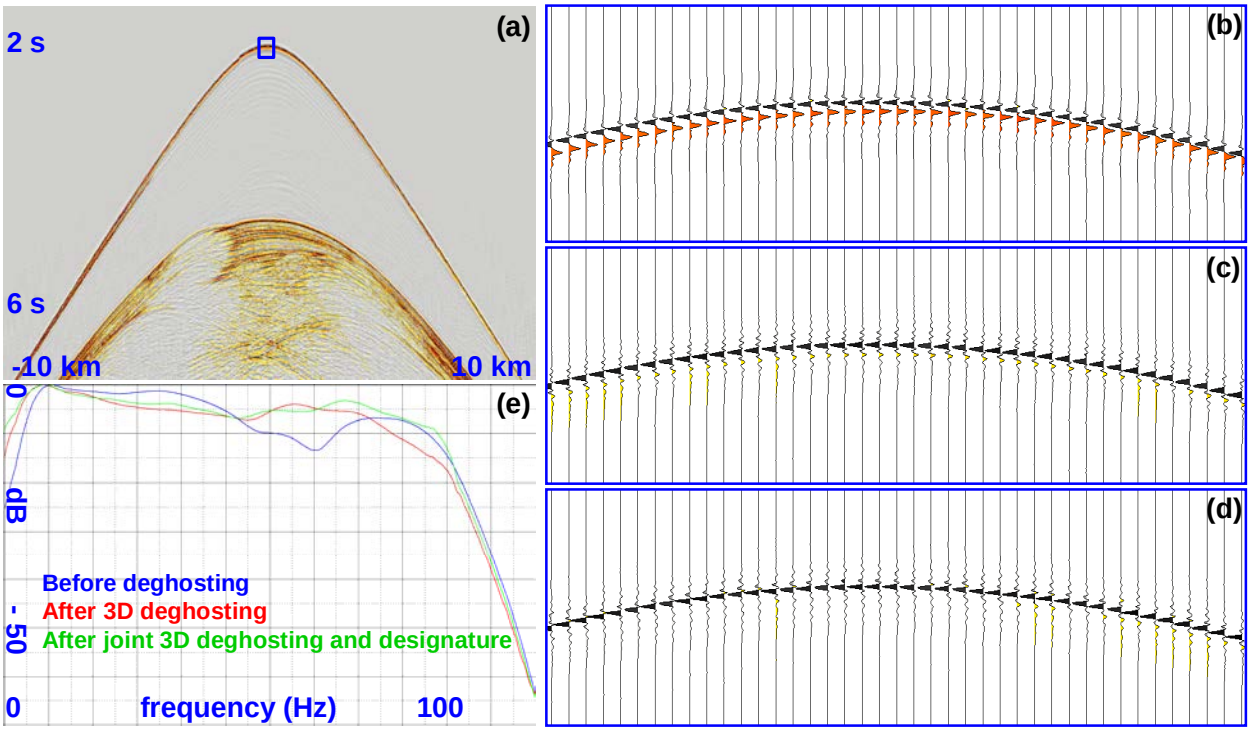

Figure 6: (a) One node gather. Wavelet view of (b) input data, (c) after 3D deghosting, and (d) after joint 3D deghosting and designature. (e) Amplitude spectrum. The blue curve is the input data, the red curve is after 3D deghosting, and the green curve is after joint 3D deghosting and designature.

DOI http://dx.doi.org/10.1190/segam2015-5924634.1

EDITED REFERENCES

Note: This reference list is a copyedited version of the reference list submitted by the author. Reference lists for the 2015 SEG Technical Program Expanded Abstracts have been copyedited so that references provided with the online metadata for each paper will achieve a high degree of linking to cited sources that appear on the Web.

REFERENCES

Kemal, A., R. Ozdemi, P. Caprioli, A. Ozebek, E. Kragh, and J. Robertsson, 2008, Optimized deghosting of over/under towed-streamer data in the presence of noise: The Leading Edge, **27**, 190–199. http://dx.doi.org/10.1190/1.2840366.

Lee, C., Y. Li, S. Ray, and G. Poole, 2014, Directional designature using a bootstrap approach: 84th Annual International Meeting, SEG, Expanded Abstracts, 4253–4257.

Poole, G., 2013, Premigration receiver deghosting and redatuming for variable depth streamer data: 83rd Annual International Meeting, SEG, Expanded Abstracts, 4216–4220.

Poole, G., and C. Davison, 2013, Shot-to-shot directional designature using near-field hydrophone data: 83rd Annual International Meeting, SEG, Expanded Abstracts, 4236–4240.

Poole, G., C. Davison, J. Deeds, K. Davies, and G. Hampson, 2013, Shot-to-shot directional designature using near-field hydrophone data: 83rd Annual International Meeting, SEG, Expanded Abstracts, 4236–4240.

Riyanti, C., R. van Borselen, P. van den Bert, and J. Fokkema, 2008, Pressure wavefield deghosting for nonhorizontal streamers: 78th Annual International Meeting, SEG, Expanded Abstracts, 2652–2656.

Wang, P., S. Ray, and K. Nimsaila, 2014, 3D joint deghosting and crossline interpolation for marine single-component streamer data: 84th Annual International Meeting, SEG, Expanded Abstracts, 3594–3598.

Wang, P., S. Ray, C. Peng, Y. Li, and G. Poole, 2013, Premigration deghosting for marine streamer data using a bootstrap approach in tau-p domain: 75th Annual International Conference and Exhibition, EAGE, Extended Abstracts, 4221–4225.

Wang, P., K. Nimsaila, D. P. Zhuang, Z. Fu, H. Shen, and G. Poole, 2015, Joint 3D source-side deghosting and designature for modern air-gun arrays: Presented at the 77th Annual International Conference and Exhibition, EAGE.

Wu, Q. F., C. C. Lee, W. Zhao, P. Wang, and Y. Li, 2014, 3D deghosting for full-azimuth and ultra-long offset marine data: 84th Annual International Meeting, SEG, Expanded Abstracts, 4238–4242.

Ziolkowski, A., G. E. Parkes, L. Hatton, and T. Haugland, 1982, The signature of an air-gun array: computation from near-field measurements including interactions: Geophysics, **47**, 1413–1421. http://dx.doi.org/10.1190/1.1441289.

DOI http://dx.doi.org/10.1190/segam2015-5924634.1